IET Electric Power Applications

Research Article

IET Journals
The Institution of Engineering and Technology

Induction motor fault detection based on multi-sensory control and wavelet analysis

ISSN 1751-8660
Received on 13th January 2020
Revised 17th June 2020
Accepted on 30th June 2020
E-First on 14th August 2020
doi: 10.1049/iet-epa.2020.0030
www.ietdl.org

Ukashatu Abubakar[1,2], Saad Mekhilef[1,3,4] ✉, Khalaf S. Gaeid[5], Hazlie Mokhlis[2], Yousif I. Al Mashhadany[6]

[1]*Power Electronics and Renewable Energy Research Laboratory (PEARL), Department of Electrical Engineering, University of Malaya 50603 Kuala Lumpur, Malaysia*

[2]*Department of Electrical Engineering, University of Malaya, 50603 Kuala Lumpur, Malaysia*

[3]*Center of Research Excellence in Renewable Energy and Power Systems, King Abdulaziz University, Jeddah 21589, Saudi Arabia*

[4]*School of Software and Electrical Engineering, Swinburne University, Victoria, Australia*

[5]*Department of Electrical Engineering, Tikrit University, Tikrit City, Iraq*

[6]*Department of Electrical Engineering, University of Anbar, Ramadi City, Iraq*

✉ *E-mail: saad@um.edu.my*

Abstract: Detection and fault-tolerant control (FTC) of faults in the early stage is desirable in improving efficiency. An implementation strategy is proposed for the individual controllers that work collectively in induction motor (IM) drive by interswitching from one form of a control strategy to another. The interswitching occurs between voltage by frequency (V/f) open-loop control, closed-loop (V/f) control, sensorless vector control and sensor vector control. Optimal performance capabilities are attained with vector control, whereas V/f is a setup that is affordable but with increased speed. In this study, the faults are open and short circuits winding faults, speed sensor failures and stator winding faults. When the severity of the fault is high, an embedded protection entity interrupts the motor. Daubechies 10 wavelet is used due to its significant vanishing moments compared to the other types of Daubechies as fault index with the stator current of 1 kW IM. A novel enhanced model reference adaptive system is employed for sensorless vector control to assess the motor speed. Both the simulation and experiment (using the F28335 DSP controller) indicate that the framework is effective in detecting the fault, ensuring the robustness of the FTC scheme and proving the effectiveness of the proposed algorithm.

Nomenclature

db10	Daubechies 10 wavelet
W_{index}	wavelet index
a	scaling parameter
b	localisation factor
x_{h}	high-frequency band limit
x_{l}	low-frequency band limit
$E_{(\text{S})}$	Shannon entropy
f	fundamental frequency
w	width or window
$S_{(n)}$	partial sum sequence entropy
Ψ	mother/original wavelet
x	time in wavelet analysis
$L_2(R)$	multiresolution frame
T_{e}	electrical torque
p	number of poles
v/f	voltage/frequency
d - q	direct–quadrature axis orientation
v_d, v_q	direct–quadrature voltages
L_{m}	magnetising inductance
T_{s} f_{s}	sampling time and frequency
T_0 T_1 T_2	switching time duration
I_{S}	main stator current
v_{ds}, v_{qs}	stator voltages
i_{sd}, i_{sq}	stator currents
R_s, L_s	resistance and inductance of stator
$R_{\text{r}}, L_{\text{r}}$	resistance and inductance of rotor
$\lambda_{dr}, \lambda_{qr}$	rotor direct–quadrature flux linkages
$\lambda'_{dr}, \lambda'_{gr}$	referenced rotor flux linkages
$\frac{\text{d}i_{ds}}{\text{d}t}$ $\frac{\text{d}i_{qs}}{\text{d}t}$	derivatives of stator currents
σ	leakage coefficient
φ_{airgap}	airgap flux
E_{airgap}	airgap electromotive force
N	rate limiter input
t	time
δ	rising slew rate
ω_0	initial angular speed
ω_{Enhancer}	enhanced angular speed
ω, $\omega_{\text{reference}}$	original and reference angular speed
ε	speed error
$O_{\frac{O}{P}}(i)$	rate limiter output
$\propto$	angle
γ	falling slew rate
n	nth order

1 Introduction

The induction motor (IM) has been the most prominent drive employed in industrial applications and energy conversion systems for the past decades. This prominence is due to its rugged design, ease of maintenance and cost-effectiveness. During the operation of an IM, various types of faults are encountered as a result of electrical, mechanical, magnetic, thermal and environmental forces [1]. Identifying and diagnosing these faults require a combination of control and fault classification techniques for the reliable operation of the motor. The control techniques include fault-tolerant control (FTC), which is implemented concurrently with fault diagnostic methods. These methods include thermal imaging, conventional relays (current, voltage and thermal) and monitoring of mechanical vibrations. They all facilitate the FTC and help to obtain an excellent post-fault performance [2]. However, the growing number of power electronic converter applications in motor drives have rendered most of these techniques ineffectual [3]. Therefore, to improve the robustness of the motor drives, digital protection techniques are needed in motor drives.

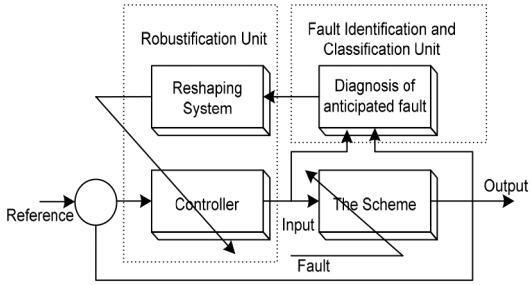

Fig. 1 *Active fault-tolerant control*

The procurement order for induction motor drives (IMDs) has spiked in the industry, due to its reliability and optimal performance. This has sparked a major research interest regarding the design of state-of-the-art controllers required for a wide range of applications. The intelligent (fuzzy logic, neural networks, genetic algorithm etc.), vector, proportional–derivative–integral, sliding mode and direct torque controllers are among the numerous controllers proposed to achieve optimal performance from motor drives [4–7]. Model predictive control (MPC) for power converters and drives can be considered as a standardised scheme for research and development. However, efforts are required to take this technology to the commercial and industrial stages. The MPC techniques are based on optimisation standards [8]. Model reference adaptive control is usually employed in machine drives, including the IM [9], to manage the speed of the motor. This is achieved by manipulating parameters such as the back-electromotive force, flux and reactive power that is naturally unaffected by the stator resistance [10]. Nonetheless, such architecture is incapable of handling the stability properly while in the regenerative mode [11].

Original works on digital protection in motor drives were established based on the electric machine models. The negative/zero sequence currents, voltages and impedance values have been used for fault detection and classification owing to their affinity towards asymmetries resulting from any fault. Potential asymmetries resulting from the framework of the controller, supply circuits and motor construction have introduced a high source of error in the classification and detection of the fault [12–16]. Other applications of automated protection employed in motor drives have been accomplished using online approximations of the motor data specifications, in which the faults are detected and classified based on variation in the magnitude of the approximated data [17]. The need for specifying threshold from faultless motor drive complicates the applications of this method in digital based scheme.

A motor current signal analysis (MCSA) strategy for detecting and diagnosing faults in the motor has been introduced to achieve improved performance due to the shortcomings of the previous techniques. This approach is developed out of the variation of magnetic flux in the motor stator current as a result of a transient fault. Protection strategies that are based on MCSA have yielded more promising results, such as their ease of implementation and minimal sensitivity to the control framework and non-linearities [18, 19].

The digital protection techniques based on harmonics have pioneered the development of the MCSA approach in motor protection with power electronic converters. In this approach, discrete Fourier transform and fast Fourier transformation (FFT) have been employed to capture selected harmonics originating from voltages and/or currents [20, 21]. This type of digital protection technique which is based on harmonics has displayed an enhanced performance compared with over-current protection techniques. However, this protection technique has some shortcomings in high-performance drives applications because of the harmonics injected by the power electronic converters. Furthermore, the non-periodic and non-stationary features of transient disturbances in motor drives raise some concerns regarding their online applications due to the issue of window size specifications [17].

To tackle the shortcomings of the harmonics-based digital protection, the MCSA is proposed using the paradigm of pattern recognition. The digital protection based on artificial neural network (ANN) is realised and applied in motor drives (induction and permanent magnet). The standard framework of ANN needed to train the ANN for online deployment, together with the requirement for data mining, has presented a major problem for implementing the artificial intelligence-based protection technique in IMDs [22, 23]. Recently, the MCSA strategy has been achieved by the time–frequency (TF) study. Usually, minimal sensitivities to a slight alteration in the motor specification and control architecture are achieved, and almost independent to window size for online implementation when TF-based digital protection is employed. The applications of wavelet transform such as discrete wavelet transform (DWT), continuous wavelet transform [24] and wavelet packet transform (WPT) in motor drives and power converters protection have received tremendous attention in power system and renewable energy systems. This is because of wavelet capacity, especially the WPT, to precisely localise the faulty signal with structures of complex TF nature. The faulty signal mostly emanates from transient fault encountered by the IM [25].

In the multi-phase machines, FTC can manage the single-phase or adjacent double-phase open circuit faults, and the machines can remain in operation using other healthy phases [26].

Further applications of WPT-based digital protection for IMDs involve integration into processing control stages, such as fuzzy logic and neural networks [27, 28]. The requirement for training and paradigm specification has caused a huge computational burden, which cast doubt regarding their online deployments. The performance of WPT-based digital protection proves to be outstanding, but its incorporation into IMDs has proven to be a difficult task.

The fault tolerance and robustness of multisensory protective strategy in drives, without the need for retrofitting extra hardware, can be referred to as ‘classical’ application. The interswitching ability of motor drives, due to the additional degree-of-freedom offered by more than one control technique has been an intriguing field of study. In this paper, a FTC approach that considers several IM faults is carried out, as depicted in Fig. 1. A motor drive utilising a vector control and equipped with an encoder is the primary control framework. When failure is anticipated from the encoder, the model changes to sensorless control mode. A short or open circuit in the stator winding causes the closed-loop V/f model to take over. If a fault occurs due to low voltage, the paradigm switches to open-loop V/f mode. The faults are diagnosed by the application of the wavelet index function. In case of persistent degradation in the motor performance, the protection circuit, comprising the control and the wavelet stops the motor.

The controllers guarantee the efficiency and swift response of each of the four control schemes (sensor vector, sensorless vector, closed-loop frequency to voltage and open-loop frequency to voltage control) and activate the protection scheme in the worst-case operation. The wavelet transform is demonstrated to be an efficacious fault detector and works as wavelet index for faults. In addition to that, the system is very flexible as it can revert to the principal controller, in the event that the motor recommences operation in healthy mode, thus guaranteeing its availability at every instant. Furthermore, the need for extra hardware to implement the protection circuit has been eliminated, lowering the cost of the IM drive. In addition to that, the sensorless vector control introduces a novel enhanced model reference adaptive system (EMRAS) to measure the speed. This will obviate the burden of tuning experienced in the case of proportional–integral (PI) controller implementation. These are the most important contributions of this work.

The paper outline is as follows. Commonly employed control techniques for the IM are described in Section 2, EMRAS is featured in Section 3, fault detection using the wavelet index is demonstrated in Section 4, the platform of the FTC is introduced in Section 5, results and discussion are presented in Section 6. Lastly, conclusion is given in Section 7.

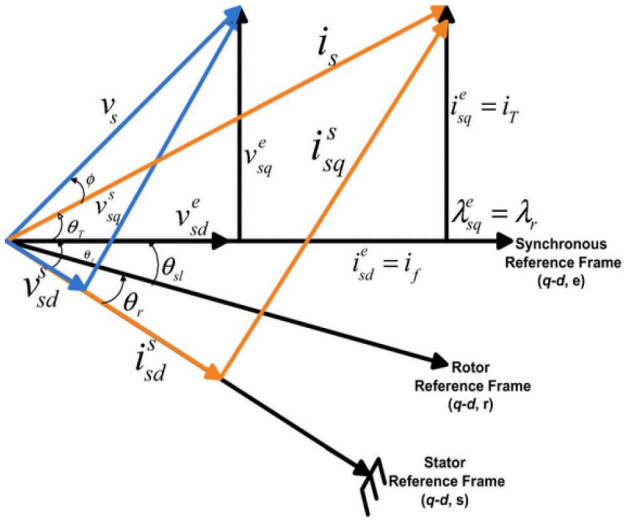

Fig. 2 *Reference frame for vector control*

2 Commonly employed control techniques for the IM

To linearly control the resulting torque from an IM drives, it is desired that the vector control decouples the torque currents and the flux, as shown in Fig. 2.

The three phases of currents and voltages are converted to two-phase dq axes. Such conversion can be expressed mathematically as a set of three-phase currents as [29]. The rotor flux space vector rotates owing to the synchronous rotation of the dq frame. The mathematical formulation of torque in an IM is given in the following equation [30]:

$$T_{\mathrm{e}} = \frac{3}{2}p\frac{L_{\mathrm{m}}}{L_{\mathrm{r}}}(\Phi_{\mathrm{r}d}i_{sq} - \Phi_{\mathrm{r}d}i_{sd}) \tag{1}$$

The sense of direction of the vectors in Fig. 2 implies that $\Phi_{\mathrm{r}d}$ becomes zero, thus the equation reduces to

$$T_{\mathrm{e}} = \frac{3}{2}p\frac{L_{\mathrm{m}}}{L_{\mathrm{r}}}(\Phi_{\mathrm{r}d}i_{sq}) \tag{2}$$

It can be deduced from (2) that the motor torque can be managed by regulating i_{sq}. Due to its ease of implementation, vector control equipped with a sensor is adopted as the main controller in this study.

The encoder employed to estimate the speed and position may give rise to some complications. Faults such as offset, distortions, losses in the resulting information, erroneous measurement and channel mismatch may occur [31, 32]. Usually, observers are required to approximate positions during the application of motor drives in sensorless vector control mode. Sensorless control simplifies complications caused by the hardware, minimises its volume, cost and maintenance. It also provides the means to bypass the problem of direct sensor wiring, thereby exhibiting better resistance to noise and extended durability [33].

When the voltage to frequency ratio is equal and kept constant, the stator flux in the motor is in proportion with the supply frequency and the applied voltage. Therefore, any variations in the frequency cause the speed to change. However when the voltage to frequency ratio is retained at an equal ratio, the torque and flux are kept constant for the entire range of speed. The speed is fine-tuned by searching for the best f, while keeping V/f constant to prevent saturation of the flux, as expressed in (3) and (4)

$$E_{\mathrm{airgap}} = kf\varphi_{\mathrm{airgap}} \tag{3}$$

Considering an unvarying air gap flux

$$E_{\mathrm{airgap}}/f \simeq v/f \tag{4}$$

Sensorless control is a straightforward control scheme. Vector control can be implemented without the need for sophisticated digital processing circuitry [32]. This special feature makes it a reliable standby control setup in anticipation of fault. Although it is commonly realised in an open loop, a closed-loop technique is also employed in higher precision applications, such as speed response estimation. To maintain the motor speed at its predetermined value, a PI controller is utilised to regulate the speed of the motor slip.

3 Enhanced model reference adaptive system

Model reference adaptive systems (MRAS) are employed to determine parameters by utilising the adaptive and reference models. The parameters to be estimated are obtained from the resulting variation of the model pair that drives the adaptive mechanism of the speed (w_0). A common constant gain linear PI regulator is usually applied by the traditional MRAS to compute the approximate speed of the rotor. The application of the PI controller resulting from the tuning is exhaustive. This study proposes the substitution of the PI controller with a 'booster or enhancer' that minimises the tuning time while offering a better response. The booster is formulated using a zero-order hold and rate limiter. Considering the scheme depicted in [33], the reference model can be represented by (5)–(9)

$$p\lambda_{\mathrm{d}r} = L_{\mathrm{r}}/L_{\mathrm{m}}(v_{ds} - \left(R_{\mathrm{s}}i_{ds} + \frac{\sigma L_{\mathrm{s}}\mathrm{d}i_{ds}}{\mathrm{d}t}\right) \tag{5}$$

$$p\lambda_{qr} = L_{\mathrm{r}}/L_{\mathrm{m}}\left(v_{qs} - \left(R_{\mathrm{s}}i_{qs} + \frac{\sigma L_{\mathrm{s}}\mathrm{d}i_{qs}}{\mathrm{d}t}\right)\right) \tag{6}$$

v_{qs} and v_{ds} are the quadratic component of stator voltage and direct component of stator voltage, respectively.

The following equations represent the adaptive model:

$$p\lambda'_{qr} = R_{\mathrm{r}}L_{\mathrm{m}}/L_{\mathrm{r}}\left(i_{qs} - \left(\frac{R_{\mathrm{r}}}{L_{\mathrm{r}}}\right)\lambda'_{qr} - \omega_0\lambda'_{\mathrm{d}r}\right) \tag{7}$$

$$p\lambda'_{\mathrm{d}r} = R_{\mathrm{r}}L_{\mathrm{m}}/L_{\mathrm{r}}\left(i_{ds} - \left(\frac{R_{\mathrm{r}}}{L_{\mathrm{r}}}\right)\lambda'_{\mathrm{d}r} - \omega_0\lambda'_{qr}\right) \tag{8}$$

The speed error (ε) is the difference between direct ($\lambda_{\mathrm{d}r}$) and quadratic (λ_{qr}) flux components of the rotor as in the following equation:

$$\varepsilon = \lambda_{qr}\lambda'_{\mathrm{d}r} - \lambda_{\mathrm{d}r}\lambda'_{qr} \tag{9}$$

where R_{s}, R_{r}, L_{r}, L_{s} and L_{m} are the rotor resistance, stator resistance, rotor inductance, stator inductance and mutual inductance, respectively.

$i_{qs}, i_{qr}, i_{\mathrm{d}r}, i_{ds}$ and p are the quadratic component of stator current, quadratic component of rotor current, a direct component of rotor current, direct component of stator current and number of pole pairs, respectively .

The error between the adaptive outputs and reference, together with the speed reference, acts as input to the booster/enhancer block depicted in Fig. 3.

The initial signals values are 0. The rate limiter regulates the variation of the signal through it by decreasing the gradient. The lower limit is referred to as falling slew parameter (γ), while the upper limit is termed the rising slew parameter (δ). The rate limiter output is computed as follows:

$$O^{o}_{\underline{p}}(i) = \nabla t\delta + N(t-1) \tag{10}$$

$$O^{o}_{\underline{p}}(i) = \nabla t\gamma + N(t-1) \tag{11}$$

$$O^{o}_{\underline{p}}(i) = N(i) \tag{12}$$

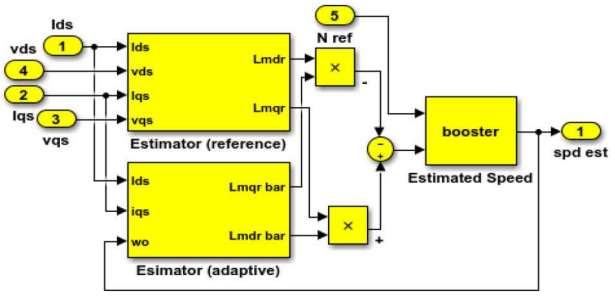

Fig. 3 *EMRAS implementation in Simulink*

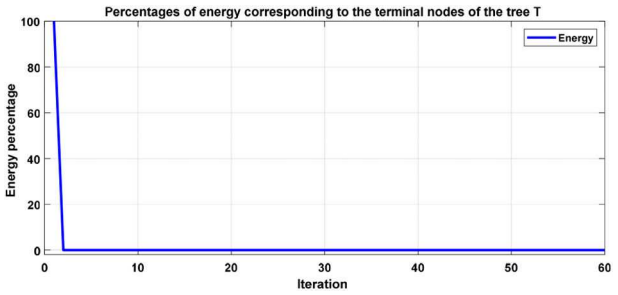

Fig. 4 *Terminal nodes and the corresponding energy proportion in percentage*

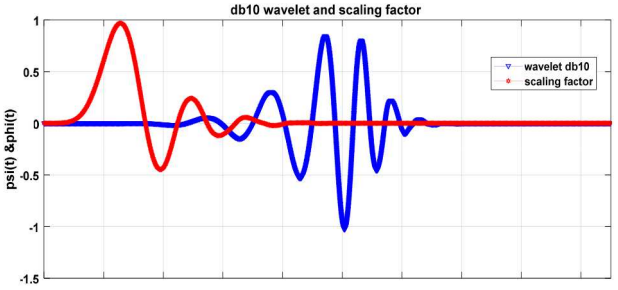

Fig. 5 *Scaling factor (red) and the Daubechies wavelet function (db10)*

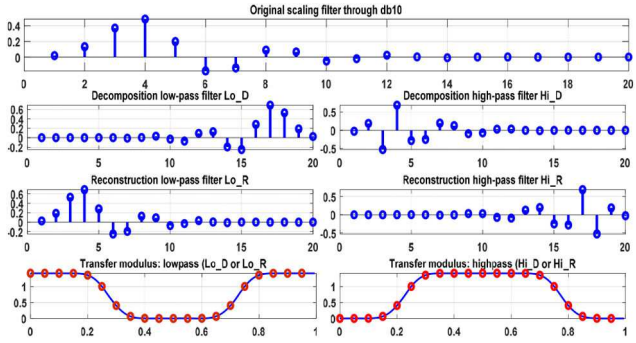

Fig. 6 *Wavelet decomposition and reconstruction*

The rate limiter input is denoted by N. The output is channelled to a zero order hold (ZOH) to form continuous time input by keeping each sample value stable over one sample period. The ZOH is analogous to a hypothetical filter that produces a piece-wise signal as expressed in the following equations:

$$o_{\mathrm{ZOH}\frac{o}{p}}(t) = \sum_{n}^{\infty} = -\infty N_{in}[n]\mathrm{rect}\left(\frac{t-nT}{T}-\frac{1}{2}\right) \tag{13}$$

Lastly, the measured speed is computed as follows:

$$\omega_{\frac{o}{p\mathrm{BMRAS}}}(i) = \omega_{\mathrm{reference}}(i) - \omega_{\mathrm{enhanced}}(i) \tag{14}$$

For (10)–(14), the rate limiter is equipped with a step solver to maintain the final output signal (error). So, if there is a difference between the lower limit and the highest value of the input signals, i.e. less than (10%), the output signal keeps increasing, regardless of all other signals.

4 Wavelet index

Wavelets are basic functions in continuous time, with localised function and zero mean. Wavelet analysis of a signal extracts essential information hidden in a signal. Wavelets possess compact support and are of orthonormal function. Thus, their coefficients can be computed from the inner product [34]. FFT produces global information (i.e. approximations) about the signal, but not local information (or details). The wavelets can precisely identify the details or the important information on a small scale, due to its localisation property. Hence, wavelets are more effective in extracting signature information present in a stationary and non-stationary signal or function compared to the FFT [34].

The stator currents of the IM drive are taken and applied to the wavelet index unit for the frequencies decomposition. The decomposition is achieved by the application of high-pass filter (HPF) an inbuilt function of the wavelet index. This HPF is utilised to capture the frequencies that are associated with fault occurrence, and are within the limits of high-frequency band classified as $x_{\mathrm{h}}: \pi/2 \leq \omega < \pi$. The frequencies that are only associated with momentary transients, i.e. resulting speed and load changes are relocated to the low-frequency band classified as $x_{\mathrm{l}}: 0 \leq \omega < \pi/2$.

Shannon entropy in (15) is used in estimating the entropy of the respective paradigm (parents) of the DWT subspace and viewing it in relation to its current (children) subspace [35]

$$E_{(\mathrm{S})} = -\sum_{n}^{N-4} S_n^2 \log\left(S_n^2\right) \tag{15}$$

where S_n is partial sum sequence of the entropy

$$\int^{\Psi}(\omega) = 0 \tag{16}$$

The following requirements are also desirable in wavelet analysis, and they motivated the selection of the optimum mother wavelet:

(a) Maximum ratio of energy/Shannon entropy
(b) Minimum Shannon entropy

To use the entropy as depicted in Fig. 4, it should have the following property: $(E(0) = 0)$.

The Daubechies 10 wavelet (db10) is selected as the appropriate mother wavelet candidate, for analysing the stator current, because of its optimal performance in the analysis of signal with discontinuities or abrupt jumps. Also, due to its significant vanishing moments, db10 can accurately detect and localised the abrupt changes and the discontinuity, which occurred during the open and short stator winding fault. Furthermore, its ease of implementation and feasibility with the DSP also makes it a best choice specifically for this application. This function is illustrated in Fig. 5. The filter decomposition and reconstruction actions to select the wavelet coefficient are shown in Fig. 6.

A criterion for the square property is required from the wavelet function so that (17) holds

$$|\Psi(\omega)|^2 = 1 \tag{17}$$

Let $\{\Psi_{a,b}(x)\}$, with $a, b \in R$ and $a \neq 0$, be a family of functions deduced from a single function $\Psi(x) \in L_2(R)$ by dilation and translation. Then, the original function Ψ expressed in (18) is typically smooth and well concentrated

$$\Psi_{a,b}(x) = \frac{1}{\sqrt{|a|}}\Psi\left(\frac{x-b}{a}\right) \tag{18}$$

If the original wavelet Ψ is centred on 0 with width w, then $\Psi_{a,b}$ is centred on b with a width aw. Parameter b represents the time

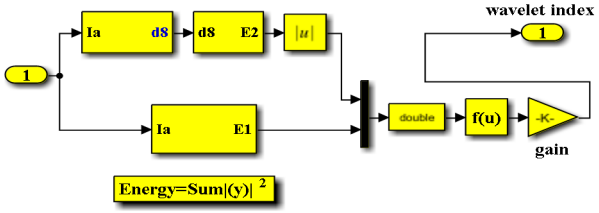

Fig. 7 *Simulink wavelet index implementation*

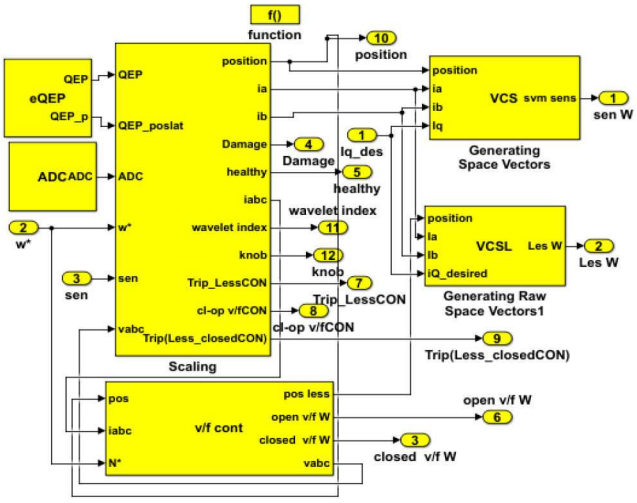

Fig. 8 *FTC algorithm*

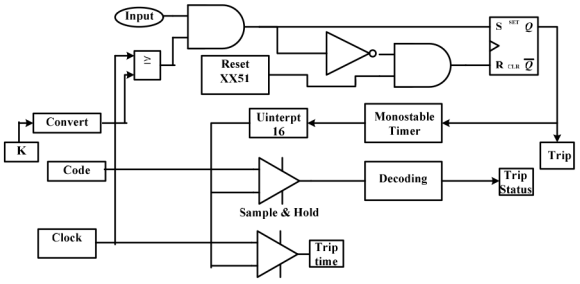

Fig. 9 *Fault detection and isolation unit implementation in Simulink*

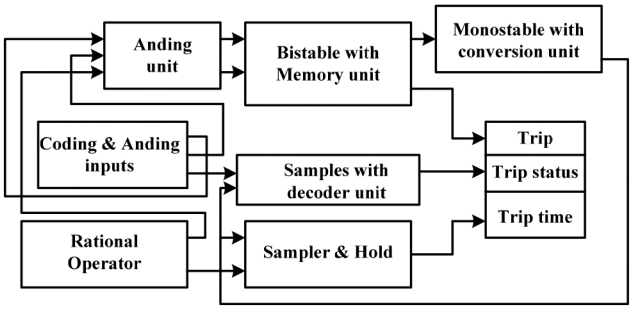

Fig. 10 *Trip data for the individual controllers executed in Simulink*

location (if x stands for time), and the scale is obtained from a. The parameter scaling is related to frequency.

In this work, the differences in the waveform of stator currents are exploited as the criterion for the fault classification. The current signal is channelled to the wavelet transform unit circuit. The valuable information is captured from the details of the sub-band signals during the processing, which is coded according to their energies. The concentration of a large amount of energy in the high-frequency sub-band of stator current can also serve as an indicator of the wavelet index. The index is determined using

$$W_{\text{index}} = \frac{\text{abs(energy}(d8))}{\text{average(energy } I_s)} \tag{19}$$

The base wavelet that possess the highest energy-to-Shannon entropy ratio is mostly selected for accurate diagnostic of the transient fault. This is because in some instances transients do occur as a result of load changes or even when the motor is starting. All these events are associated with transients but are not actually related to fault induced events. In this case, the maximum transient is arbitrarily found to be at db8 level because of its sensitivity to the transient fault variation. It is formulated together with Shannon entropy in the form of wavelet index. In this study, the condition for the actual fault occurrence is specified within the ranges of $1.35 \geq W_{\text{index}} \geq 1.3$ and $1.25 \geq W_{\text{index}}$ for the first case and the second case, respectively.

The 20 kHz sampling frequency (f_s) and the decomposition levels (L) of the wavelet can be calculated using

$$L \geq \frac{\log(f_s/f)}{\log(2)} + 1 \tag{20}$$

$$L \geq \frac{\log(2000/50)}{\log(2)} + 1 \geq 10 \tag{21}$$

In which, $d8$ represents the decomposition at the 8th level, detailed by the HPF up-sampling and down-sampling actions and considered as the direct relation between fault components and the wavelet decomposition affected level. Abs (energy ($d8$)) is used in this formula to return the absolute value of each element of the energy of the most active and sensitive level against the faults ($d8$). Thus, it implies that $d8$ possesses high sensitivity in relation to the faulty stator current. In other words, $d8$ is more sensitive to the changes of stator current parameters during the fault occurrence, or the coefficient at level $d8$ has a significant value.

The Simulink implementation is shown in Fig. 7.

5 Platform of the fault-tolerant control

One of the essential applications of FTC is in the industries operating with IM drives, especially considering the formidable costs of unintended stops of its operations. This study describes the approach of quadric-control co-working to achieve the robustification of the IM. In healthy operation, the drive is run by sensor vector control. When a fault occurs in the encoder, it switches to the sensorless mode of vector control. In the event of a short or open circuit in the stator, the scheme reverts to closed loop of V/f control mode, while open-loop V/f control mode is activated when a minimum voltage fault occurs, as shown in Fig. 8.

The diagram for the execution of one section of the fault identification and confinement unit is illustrated in Fig. 9.

The overall unit that observes the location and time of the fault occurrence in the general data recorded is depicted in Fig. 10.

The signal is compared with the reset signal through the bistable circuit. The bistable is used to store binary data utilising the characteristic of the flip-flop. The Q-state of the flip-flop is used as a latch memory for the evaluated signal to indicate the trip when the next value of the signal is different in magnitude according to the wavelet index. Monostable with two samples held within 1×10^{-9} s can recognise the trip status and trip time.

When an insignificant level of noise is erroneously diagnosed or classified as a fault, the scheme changes back swiftly to sensor mode of vector control. Lastly, the occurrence of two or more faults at once activates the protection circuit. The recommended algorithm is simulated using the digital motor control blocks, owing to its ease of compilation from C through the Texas Instruments F28335 DSP. Fig. 11 depicts its block diagram.

The FTC control switching mechanism depends on the Win to function perfectly in the right control. The vector control in the normal operation than in the closed loop or open loop in the low level of operation. The protection step would be the final step if all controllers cannot handle the operation in the satisfactory operation of the IM itself. The control scheme block diagram is shown in Fig. 12.

The detailed coefficients of the signal are generated by the application of HPFs (wavelet), while approximate coefficients of the signal are formed when the signal is passed through the low-

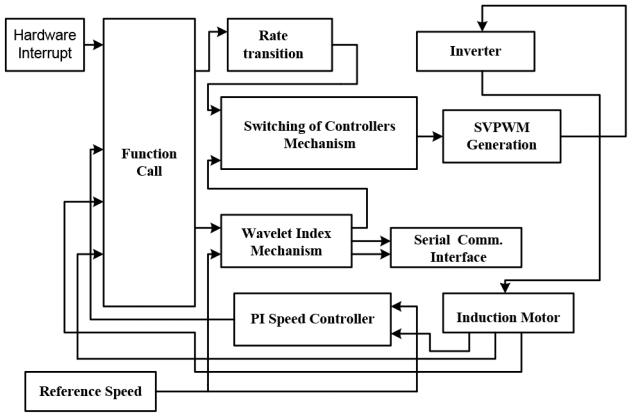

Fig. 11 *Block diagram representation of FTC scheme*

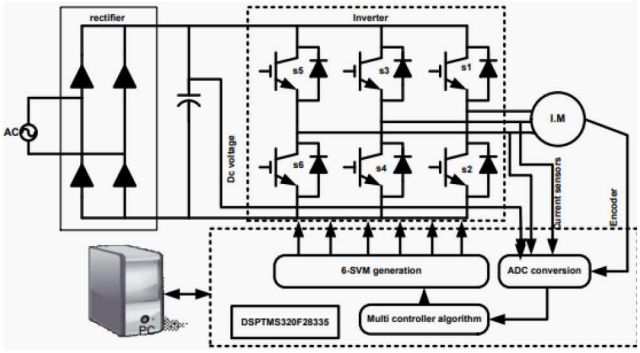

Fig. 12 *Multisensory control scheme block diagram*

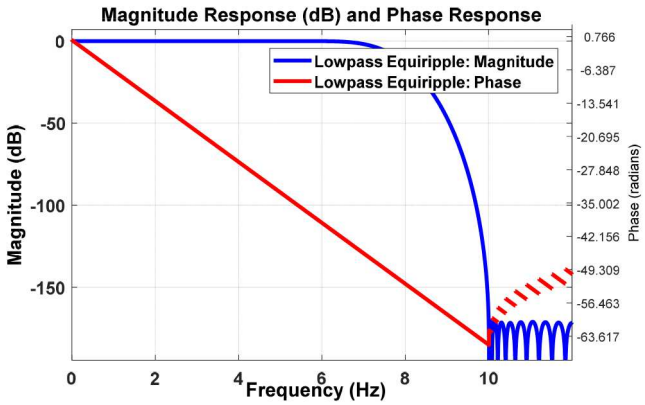

Fig. 13 *Low-pass filter (0–10) kHz magnitude and phase response*

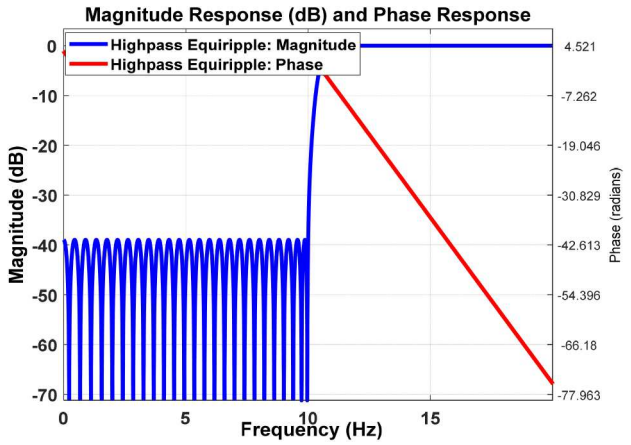

Fig. 14 *HPF (9.76–19.5313) Hz magnitude and phase response*

pass filters (scaling function). The combination of phase magnitude responses, with an impulse response of 20 kHz at each level, generates the sampling frequency. Fig. 13 shows the magnitude of the first low-pass filter implementation, while Fig. 14 shows the last magnitude and phase of HPF.

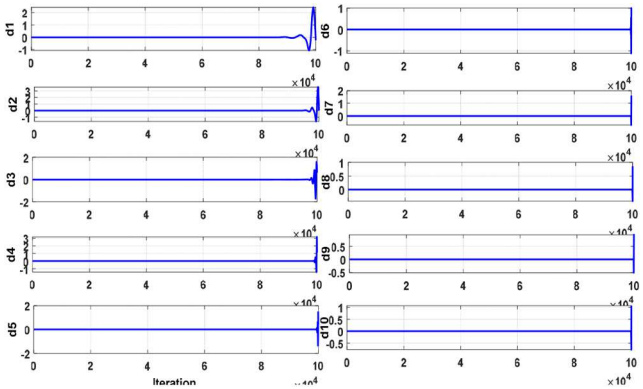

Fig. 15 *Wavelet analysis in faultless motor*

The condition for detecting a fault in an IM is among the critical stages in diagnosing the fault. The processing of the faults requires satisfying certain condition, specified by the designed wavelet index. In this case, the condition is attached directly between the wavelet index with maximum detail ($d8$) and the original stator current (I_s). This is because sub-band signal of $d8$ level conveys unique features of the original signal during the sub-band coding of the $d1$ through $d10$. The details are only obtained from the high pass sequence $dn = (d1 \ldots . d8 \ldots . d10)$, and the value coefficient at $d8$ is found to be more responsive to fault signal of stator current. This testing and checking of the detail's coefficient can be achieved heuristically or be determined using cascade algorithm.

6 Results and discussion

The backbone of the experimental outline of the IM drive is supported by DSP TMS320F28335. The processing of the stator current signal is achieved by the filter bank due to its up-sampling and down-sampling frequency of 20 kHz. The results of the healthy stator current of IM drive are presented in Fig. 15. The short momentarily spikes are not related to fault occurrence. They occurred only because of the sensitive nature of the wavelets, hence the high accuracy in classifying a fault.

The synchronisation is achieved due to the interswitching action between the exact controller that initiates the action of the wavelet index and SVM vector controller generation. Thus, the deployment of space vector PWM can be accomplished through the following equations. The derivation of voltage and angle can be achieved by

$$\begin{bmatrix} v_d \\ v_q \end{bmatrix} = \begin{bmatrix} 1 & -0.5 & -0.5 \\ 0 & \sqrt{3}/2 & -\sqrt{3}/2 \end{bmatrix} \begin{bmatrix} v_{an} \\ v_{bn} \\ v_{cn} \end{bmatrix} \tag{22}$$

The reference for the voltage equation is represented by

$$v_{\text{refer}} = \sqrt{v_q^2 + v_d^2} \tag{23}$$

The calculation of the angle is carried out using

$$\alpha = \tan^{-1}\left(\frac{v_q}{v_d}\right) \tag{24}$$

The time span can be computed in accordance with the expressions below:

$$T_1 = T_2 a \frac{\sin((\pi/3) - \alpha)}{\sin(\pi/3)} \tag{25}$$

$$a = \frac{|v_{\text{refer}}|}{2/3 v_{\text{dc}}} \tag{26}$$

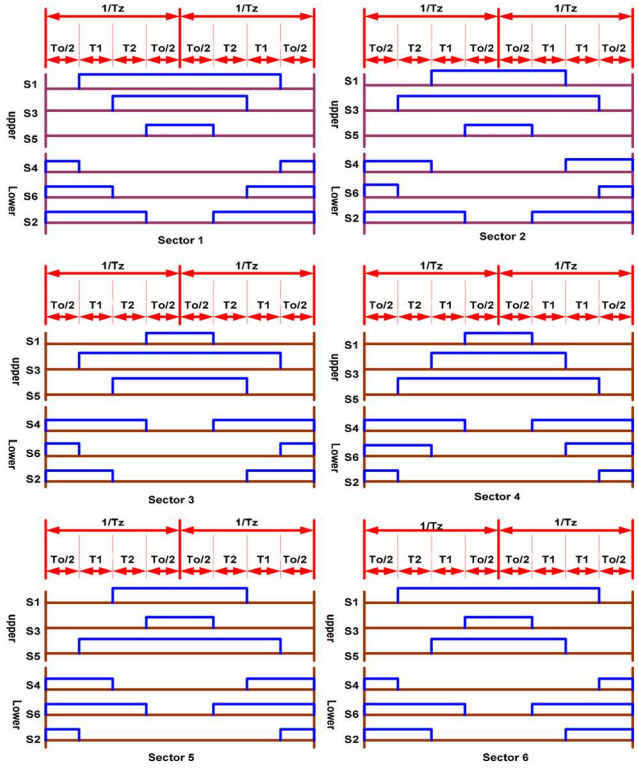

Fig. 16 *Switching fashion for the space vector PWM*

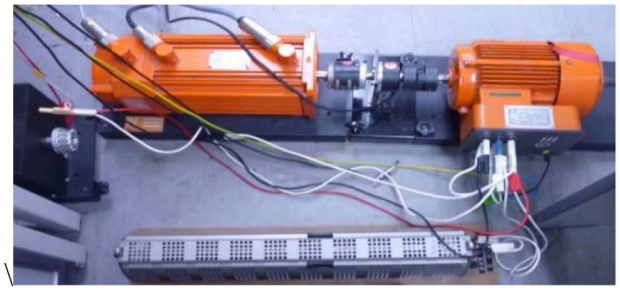

Fig. 17 *Laboratory setup to analyse the short-circuit fault in the stator with wavelet index*

$$T_z = \frac{1}{f_z} \tag{27}$$

$$T_2 = T_z a \frac{\sin(\alpha)}{\sin(\pi/3)} \tag{28}$$

$$T_0 = T_z - (T_1 + T_2) \tag{29}$$

The switching time for the six portions can be measured, as depicted in Fig. 16.

The deployment of the experimental setup of the FTC control involves the execution of the algorithm associated with fault-tolerant controller with the support of DSP TMS320F28335. Moreover, RS232 is extended to interconnect the PC and the TMS320F28335 DSP. Readings from the outputs were collected via the serial communication interface. The measurement of the stator current and the speed of the rotor were performed with the aid of ADC, at a sampling rate of 20 kHz. The application of the current sensor, which employs the principle of closed-loop Hall effect assured the safety appliance of 3 V maximal to the DSP. A signal parameterisation circuit was utilised to guarantee the regulation of the transmitted signal by the encoder to the 3 V F28335 DSP. The circuit was retrofitted and applied to initially receive the signal emanating from the encoder. Both the normal and faulty cases were studied while conducting the experiment. Additionally, open winding, sensor fault, short winding in the stator and minimum voltage were examined. The compilation and

Fig. 18 *Laboratory procedure for assessing the open-circuit fault in the stator, with wavelet index*

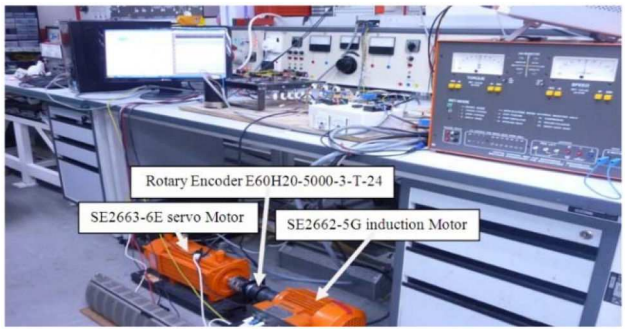

Fig. 19 *IM setup*

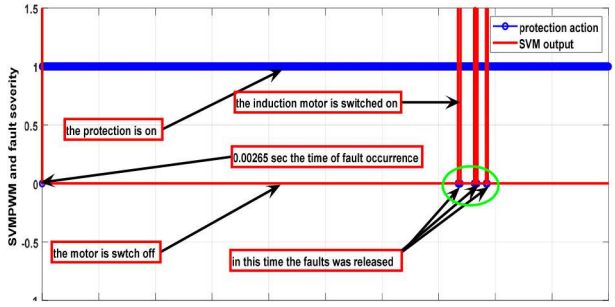

Fig. 20 *Speed difference with the binary indication*

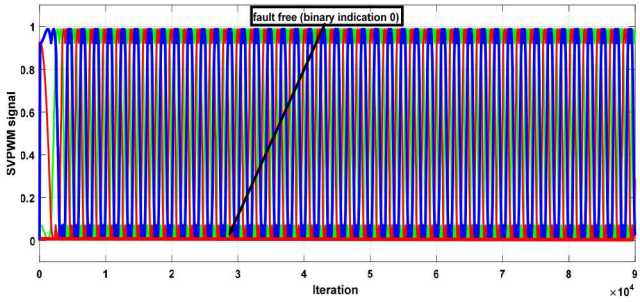

Fig. 21 *SVM control signal with 0 binary indication in healthy IM*

implementation of the FTC circuit were performed exclusively by the DSP F28335 controller and MATLAB Simulink, respectively. This is because of the matched compatibility. The laboratory equipment required for the experiment to apply the wavelet index in order to detect and evaluate the short-circuit fault in the stator of the motor is demonstrated in Fig. 17.

The laboratory layout for analysing open-circuit fault in the IM stator winding with wavelet index is illustrated in Fig. 18.

The experimental setup is depicted in Fig. 19.

The experimental study is based on two basic scenarios to examine the faulty and normal operations of the IM drives (Fig. 20). The open circuit in the stator winding, sensor fault, short-circuit in the stator winding and minimum voltage were all analysed. The compilation of FTC after its implementation with MATLAB Simulink was achieved by the DSP F28335 controller. These can be seen in the experimental procedure illustrated in Fig. 21. IEEE standards for most of the IM faults are included

Table 1 IEEE standard for observing the parameters of IM

Report of fault monitoring of an IM		
Faults	Acceptable values	Values limits
AC over current	twice rated	1.5 rated
AC under voltage	5–25% PNDA and PNDI	up to 40%
AC overvoltage	$\pm 10\%$	$\pm 10\%$
unbalance AC voltage	IEEE stand of $1-5\%$	$1-3\%$
overvoltage due to DC	V_{dc}	V_{dc}
high speed	$+25\%$	$+10\%$
low speed	-25%	-10%
broken rotor bar	for 2 poles is $20\% < 2$ m	for 2 poles is $20\% < 2$ m
stator short-winding	for 2 poles is $10\% < 2$ m	for 2 poles is $10\% < 2$ m
destruction	denied	denied

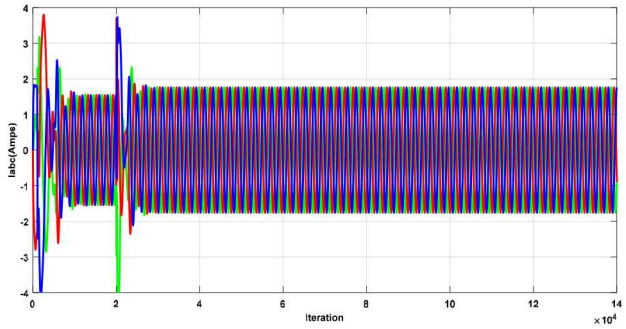

Fig. 22 *Stator current with fault injection at t = 2 s*

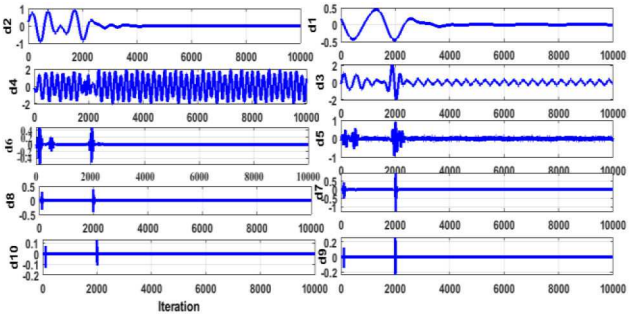

Fig. 23 *Wavelet decomposition at t = 2 s*

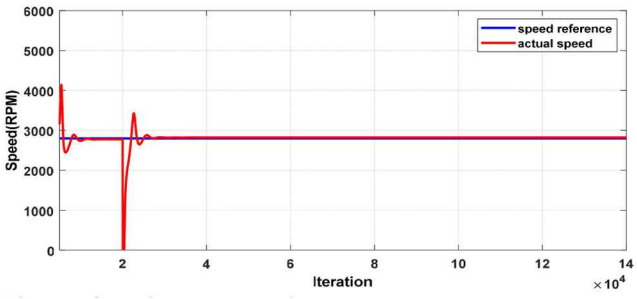

Fig. 24 *Speed reaction and recovery time*

(even though some of them are not covered in this work) to serve as a useful reference for the readers (Table 1).

They were adopted as the criteria for monitoring the parameters.

If the difference between the reference and actual speed exceeds 10%, a logic 1 appears to choose the sensorless vector control. When there is a variation of <10%, it maintains the normal operation, with the logic 0 as in Fig. 21.

The waveform of the current that represent the short-circuit fault occurrence at the instance, $t = 2$ s is presented in Fig. 22.

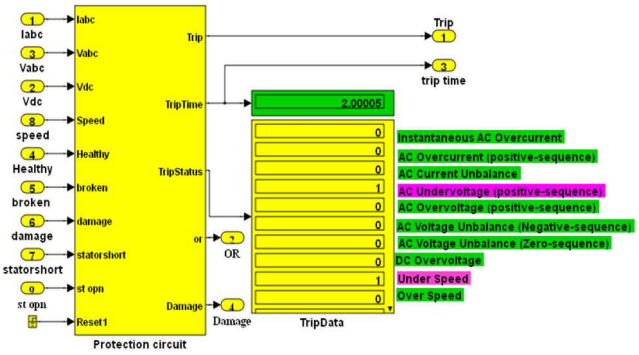

Fig. 25 *Monitoring outputs for faults at 2 s*

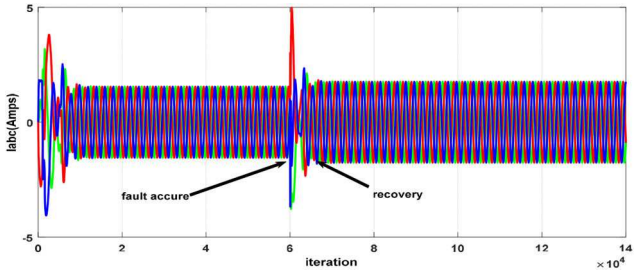

Fig. 26 *Stator current with fault injection at t = 6 s*

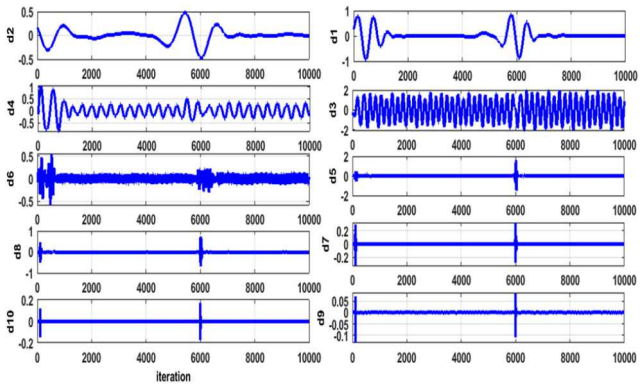

Fig. 27 *Wavelet decomposition at t = 6 s*

The corresponding wavelet waveform and the speed recovery are depicted in Figs. 23 and 24, respectively (Fig. 25).

Current waveform of the faulty system at $t = 6$ s with its corresponding wavelet is presented in Figs. 26 and 27, respectively.

The transient response and injection of stator open winding faults at 6 s are so clear in the decomposition of stator current wavelet. The speed recovery is quite clear after applying the FTC algorithm.

An open-circuit fault and short-circuit fault were generated for the period of 1.4 s and 1.12, respectively, in the stator winding in order to assess the mobility and compatibility of the algorithm compiled by the fault-tolerant controller. It was observed that the restoration time for the open-circuit fault is less than the restoration time for the short-circuit fault in the IM drive (Fig. 28).

The objective of this test is to study the degree-of-freedom of the algorithm supporting the FTC and its mobility to retreat to the sensor vector mode control. The open- and short-circuit faults were initiated concurrently in the stator winding by disconnecting one of the windings in the stator's phase and activating a solid-state switch across any of the desired phases of the stator, respectively. The faults were injected in the scheme at 1.16 s to observe the operation of the IM drive, which was found to be stopping when the protection unit takes over from the fault-tolerant algorithm.

On the other hand, the controller exits from the protective control mode and shifts to the sensor mode vector control and vice versa, as the injected fault is mitigated in a period of 1.48 s. Fig. 29 shows the simulated result.

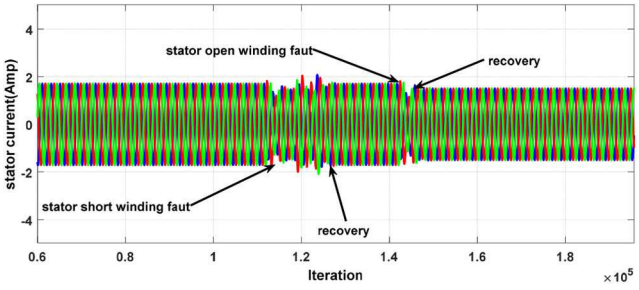

Fig. 28 *Multiple faults at different times*

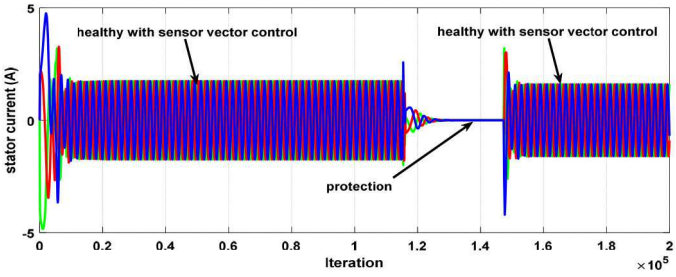

Fig. 29 *Stator current*

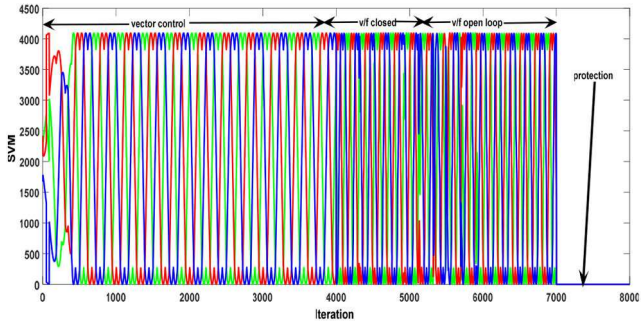

Fig. 30 *Different control*

Table 2 Parameters of the IM

Motor parameters	Rating
current	2.5 A
voltage	400 V
power	1 kW
speed	2780 rpm
no. of poles	2
R_s	20.9 Ω
R_r	19.5 Ω
L_s	0.05 H
L_r	0.05 H

Lastly, the three individual fault events, namely, the minimal voltage, open and short stator winding faults, are simulated. The minimum possible voltage is attained by decreasing the source voltage below the 200 V requirement. During the starting period of the motor, its operation was found to be normal. Subsequently, open and short winding faults occurred at two distinct time durations, i.e. at 4 s. The voltage is then decreased to a value lower than 200 V for the purpose of simulating the third fault for the duration of 5 s. Then both the open winding and reduced voltage were applied at 7 s. Consequently, at the time the vector control was commanding, the V/F control mode takes charge after 4 s in order to remedy the short or open winding faults in the stator. This multisensory control technique changed over to open mode of V/F control to offset the last fault and regulate the IM drive operation with negligible distortion. In case of a severe fault, the protection circuit is energised to interrupt the running motor (Fig. 30).

The derivation of the mathematical relationship between the designed wavelet index and the overall effect of stator resistance is instrumental for the intervals in the wavelet index. The expression for the wavelet index at 1600 rpm with a curve fitting is linearly represented as

$$W_{\text{ind}} = 0.0217 \times R_{\text{Shunt effect}} + 1.796 \tag{30}$$

The linear curve fitting with a 900 rpm wavelet index can be expressed as

$$W_{\text{ind}} = 0.0843 \times R_{\text{shunt effect}} + 1.782 \tag{31}$$

The linear curve fitting equation having 400 rpm wavelet indicator is

$$W_{\text{ind}} = 0.0986 \times R_{\text{shunt effect}} + 1.146 \tag{32}$$

The linear curve that fits the open winding of the stator and a wavelet ratio of 1600 RPM is

$$W_{\text{ind}} = 0.00919 \times R_{\text{series effect}} + 1.369 \tag{33}$$

The linear equation which fits a curve in the stator open winding, and with 900 rpm wavelet indicator is expressed as

$$W_{\text{ind}} = 0.0084 \times R_{\text{series effect}} + 1.257 \tag{34}$$

The linear curve fitting equation of the stator open winding having a 450 rpm wavelet index ratio is

$$W_{\text{ind}} = 0.0024 \times R_{\text{series effect}} + 0.943 \tag{35}$$

The relationship is obtained experimentally by inserting a series or parallel resistance with stator resistance to test the open or short winding faults, and at each instance the Win is recorded (Table 2). The results are stored in the PC, and the mathematical formulae could be obtained using the MATLAB identification toolbox (Figs. 31 and 32).

7 Conclusions

In this work, a wavelet-based FTC for IM is developed. This is achieved through a multisensory control strategy (sensor and sensorless vector control and open-loop and closed-loop V/f) that interoperates between the individual controller to remedy or

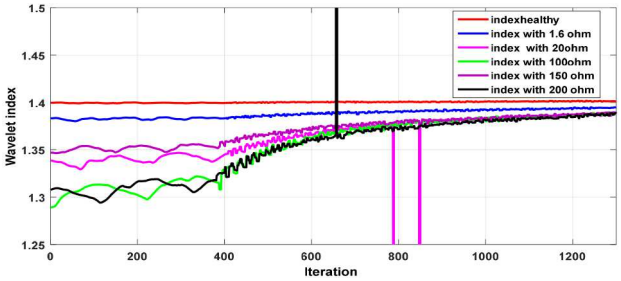

Fig. 31 *Different values of wavelet index correspond to stator resistance*

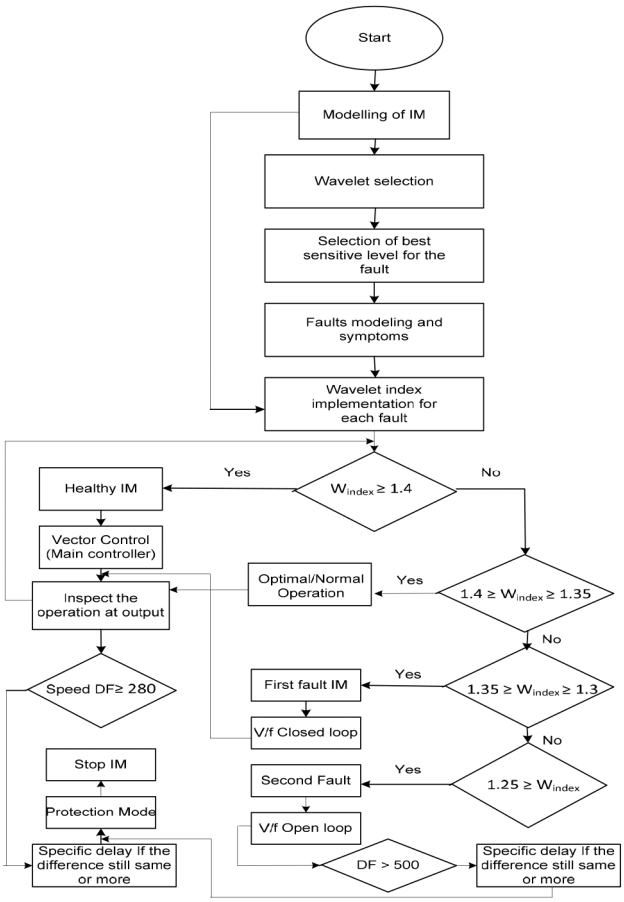

Fig. 32 *Flowchart of the complete work*

circumvent the anticipated fault. Furthermore, a protection unit that utilises the wavelet index in classifying and detecting the faults is retrofitted. This has the advantage of minimal sensitivity to the loading level, location and type of faults. This distinct feature of the wavelet makes it an accurate tool for diagnosing a fault in motor drives, including the IM because it can distinguish between the transient response from the speed or load changes and the actual occurrence of the real fault. In addition to that, FTC and protection techniques were developed based on the motor electrical parameters, such as rotor/stator voltage or current, to minimise the complexity of the monitoring scheme. This approach further improves the ruggedness of the motor and hence its reliability, with the DSP F28335 controller as a new trend in the verification of the proposed algorithm.

8 Acknowledgments

The authors would like to thank University of Malaya, Malaysia, for providing financial support under the research grant Impact Oriented Interdisciplinary Research Grant (IIRG) IIRG011A-2019, Ministry of Higher Education Malaysia, under Large Research Grant Scheme (LRGS) LR008-2019 and Ministry of International Trade and Industry (MITI) Malaysia through MIDF under High Value Added and Complex Product Development and Market Program: GA016-2019.

9 References

[1] Hassan, O.E., Amer, M., Abdelsalam, A.K., *et al.*: 'Induction motor broken rotor bar fault detection techniques based on fault signature analysis–a review', *IET Electr. Power Appl.*, 2018, **12**, (7), pp. 895–907

[2] Zhang, J., Zhan, W., Ehsani, M.J.I.T.O.E.C.: 'Fault-tolerant control of PMSM with inter-turn short-circuit fault', *IEEE Trans. Energy Convers.*, 2019, **34**, (4), pp. 2267–2275

[3] Amini, J., Moallem, M.J.I.T.O.I.E.: 'A fault-diagnosis and fault-tolerant control scheme for flying capacitor multilevel inverters', *IEEE Trans. Ind. Electron.*, 2016, **64**, (3), pp. 1818–1826

[4] Farah, N., Talib, M.H.N., Mohd Shah, N.S., *et al.* 'A novel self-tuning fuzzy logic controller based induction motor drive system: an Experimental approach', *IEEE Access*, 2019, **7**, pp. 68172–68184

[5] Lee, J.-H., Pack, J.-H., Lee, I.-S.J.A.S.: 'Fault diagnosis of induction motor using convolutional neural network', *Appl. Sci.*, 2019, **9**, (15), p. 2950

[6] Jiang, D., Yu, W., Wang, J., *et al.*: 'A speed disturbance control method based on sliding mode control of permanent magnet synchronous linear motor', *IEEE Access*, 2019, **7**, pp. 82424–82433

[7] Barrero, F., Duran, M.J.J.I.T.O.I.E.: 'Recent advances in the design, modeling, and control of multiphase machines—part I', *IEEE Trans. Ind. Electron.*, 2015, **63**, (1), pp. 449–458

[8] Vazquez, S., Rodriguez, J., Rivera, M., *et al.*: 'Model predictive control for power converters and drives: advances and trends', *IEEE Trans. Ind. Electron.*, 2016, **64**, (2), pp. 935–947

[9] Fei, Q., Deng, Y., Li, H., *et al.*: 'Speed ripple minimization of permanent magnet synchronous motor based on model predictive and iterative learning controls', *IEEE Access*, 2019, **7**, pp. 31791–31800

[10] Teja, A.R., Verma, V., Chakraborty, C.J.I.T.O.I.E.: 'A new formulation of reactive-power-based model reference adaptive system for sensorless induction motor drive', *IEEE Trans. Ind. Electron.*, 2015, **62**, (11), pp. 6797–6808

[11] Seshadrinath, J., Singh, B., Panigrahi, B.K.J.I.T.O.I.I.: 'Vibration analysis based interturn fault diagnosis in induction machines', *IEEE Trans. Ind. Inf.*, 2013, **10**, (1), pp. 340–350

[12] Gonzalez-Prieto, I., Duran, M., Bermúdez, M., *et al.*: 'Assessment of virtual-voltage-based model predictive controllers in six-phase drives under open-phase faults', *IEEE J. Emerging Sel. Topics Power Electron.*, 2019, p. 1

[13] Duran, M.J., Barrero, F.J.I.T.O.I.E.: 'Recent advances in the design, modeling, and control of multiphase machines—part II', *IEEE Trans. Ind. Electron.*, 2015, **63**, (1), pp. 459–468

[14] Saleh, S., Ozkop, E.J.I.T.O.I.A.: 'Phaselet-based method for detecting electric faults in 3ϕ induction motor drives—part II: performance evaluation', *IEEE Trans. Ind. Appl.*, 2016, **53**, (3), pp. 2988–2996

[15] Saleh, S.A., Ozkop, E., Aljankawey, A.S.J.I.T.O.I.A.: 'Performance of the phaselet frames-based digital protection for distributed generation units', *IEEE Trans. Ind. Appl.*, 2015, **52**, (3), pp. 2095–2109

[16] Stojčić, G., Pašanbegović, K., Wolbank, T.M.: 'Detecting faults in doubly fed induction generator by rotor side transient current measurement', *IEEE Trans. Ind. Appl.*, 2014, **50**, (5), pp. 3494–3502

[17] Gyftakis, K.N., Antonino-Daviu, J.A., Garcia-Hernandez, R., *et al.*: 'Comparative experimental investigation of broken bar fault detectability in induction motors', *IEEE Trans. Ind. Appl.*, 2015, **52**, (2), pp. 1452–1459

[18] Ali, M.Z., Shabbir, M.N.S.K., Liang, X., *et al.*: 'Machine learning-based fault diagnosis for single-and multi-faults in induction motors using measured stator currents and vibration signals', *IEEE Trans. Ind. Appl.*, 2019, **55**, (3), pp. 2378–2391

[19] Antonino-Daviu, J., Popaleny, P.: 'Detection of induction motor coupling unbalanced and misalignment via advanced transient current signature analysis'. 2018 XIII Int. Conf. on Electrical Machines (ICEM), Alexandropoulos, Greece, 2018, pp. 2359–2364

[20] Bessous, N., Zouzou, S., Bentrah, W., *et al.*: 'Diagnosis of bearing defects in induction motors using discrete wavelet transform', *Int. J. Syst. Assurance Eng. Manage.*, 2018, **9**, (2), pp. 335–343

[21] Samaga, B.R., Vittal, K.J.I.J.O.E.P., Systems, E.: 'Comprehensive study of mixed eccentricity fault diagnosis in induction motors using signature analysis', *Int. J. Electr. Power Energy Syst.*, 2012, **35**, (1), pp. 180–185

[22] Gowthami, K., Kalaivani, L.: 'Fault classification of induction motor bearing using adaptive neuro fuzzy inference system'. 2019 Fifth Int. Conf. on Electrical Energy Systems (ICEES), Chennai, India, 2019, pp. 1–6

[23] Zolfaghari, S., Noor, S.B.M., Rezazadeh Mehrjou, M., *et al.*: 'Broken rotor bar fault detection and classification using wavelet packet signature analysis based on Fourier transform and multi-layer perceptron neural network', *Appl. Sci.*, 2018, **8**, (1), p. 25

[24] Rangel-Magdaleno, J., Peregrina-Barreto, H., Ramirez-Cortes, J., *et al.*: 'Vibration analysis of partially damaged rotor bar in induction motor under different load condition using DWT', *Shock Vib.*, 2016, **2016**, pp. 1–11doi:

[25] Abid, F.B., Zgarni, S., Braham, A.J.I.T.O.E.C.: 'Distinct bearing faults detection in induction motor by a hybrid optimized SWPT and aiNet-DAG SVM', *IEEE Trans. Energy Convers.*, 2018, **33**, (4), pp. 1692–1699

[26] Rangari, S.C., Suryawanshi, H.M., Renge, M.J.E.: 'New fault-tolerant control strategy of five-phase induction motor with four-phase and three-phase modes of operation', *Electronics. (Basel)*, 2018, **7**, (9), p. 159

[27] Ammar, A.J.C.-T.I.J.F.C., Electrical, M.I., Engineering, E.: 'Performance improvement of direct torque control for induction motor drive via fuzzy logic-feedback linearization', *Int. J. Comput. Math. Electr. Electron. Eng.*, 2019, **38**, pp. 672–692

[28] Nayak, J., Naik, B., Pelusi, D.*, et al.*: 'A comprehensive review and performance analysis of firefly algorithm for artificial neural networks'. *Nature-Inspired Comput. Data Mining Machine Learning*, 2020, **855**, p. 137
[29] Saleh, S., Ozkop, E.J.I.T.O.I.A.: 'Phaselet-based method for detecting electric faults in 3ϕ induction motor drives—part I: analysis and development', *IEEE Trans. Ind. Electron.*, 2016, **53**, (3), pp. 2976–2987
[30] Odhano, S.A., Bojoi, R., Boglietti, A.*, et al.*: 'Maximum efficiency per torque direct flux vector control of induction motor drives', *IEEE Trans. Ind. Appl.*, 2015, **51**, (6), pp. 4415–4424
[31] Zaky, M.S.J.I.T.O.I.E.: 'Stability analysis of speed and stator resistance estimators for sensorless induction motor drives', *IEEE Trans. Ind. Electron.*, 2011, **59**, (2), pp. 858–870
[32] dos Santos, T.H., Goedtel, A., da Silva, S.A.O.*, et al.*: 'Scalar control of an induction motor using a neural sensorless technique', *Electr. Power Syst. Res.*, 2014, **108**, pp. 322–330
[33] Ammar, A., Bourek, A., Benakcha, A.*, et al.*: 'Sensorless stator field oriented-direct torque control with SVM for induction motor based on MRAS and fuzzy logic regulation'. 2017 6th Int. Conf. on Systems and Control (ICSC), Batna, Algeria, 2017, pp. 156–161
[34] Houtveen, J.H., Molenaar, P.C.J.P.: 'Comparison between the Fourier and wavelet methods of spectral analysis applied to stationary and nonstationary heart period data', *Psychophysiology*, 2011, **38**, (5), pp. 729–735
[35] Strang, G., Nguyen, T.: 'Wavelets and filter banks', *SIAM*, 1996